Article:
Wakamoto, T., Ikeya, T., Kitazawa, S. et al. (2019) Paramagnetic relaxation enhancement-assisted structural characterization of a partially disordered conformation of ubiquitin. Protein Science, 28 (11). pp. 1993-2003. ISSN: 0961-8368

https://doi.org/10.1002/pro.3734

Full Length Article

Paramagnetic relaxation enhancement-assisted structural characterization of a partially disordered conformation of ubiquitin

Takuro Wakamoto[1], Teppei Ikeya[2], Soichiro Kitazawa[3], Nicola J. Baxter[4], Mike P. Williamson[4] and Ryo Kitahara[1,3*]

Affiliations:

[1]Graduate School of Life Sciences, Ritsumeikan University, 1-1-1 Nojihigashi, Kusatsu, Shiga 525-8577, Japan.

[2]Tokyo Metropolitan University, 1-1 Minami-ohsawa, Hachioji, Tokyo 192-0397

[3]College of Pharmaceutical Sciences, Ritsumeikan University, 1-1-1 Nojihigashi, Kusatsu, Shiga 525-8577, Japan.

[4]Department of Molecular Biology and Biotechnology, University of Sheffield, Firth Court, Western Bank, Sheffield S10 2TN, United Kingdom.

Corresponding author*: Ryo Kitahara
E-mail: ryo@ph.ritsumei.ac.jp
Tel: +81-77-561-5751, Fax: +81-77-561-2564
ORCID ID: orcid.org/0000-0003-1815-3227
Running title: PRE-assisted structural determination
Manuscript pages: 21
Supplementary material: Figure S1-S9, Methods

Abstract

Nuclear magnetic resonance (NMR) is a powerful tool to study three-dimensional structures as well as protein conformational fluctuations in solution, but it is compromised by increases in peak widths and missing signals. We previously reported that some amide group signals of residues 33–41 of ubiquitin at pH 4.5 and 273 K almost disappeared above 3 kbar. Thus, well-converged structural models could not be obtained for this region owing to the absence of distance restraints. Here, we re-examine. the problem using the ubiquitin Q41N variant as a model for this locally disordered N_2 state (N_3). We demonstrate that the variant shows pressure-induced loss of backbone amide group signals at residues 28, 33, 36, and 39–41 like the wild-type, with a similar but smaller effect on CαH and CβH signals. In order to characterise this N_3 structure, we measured paramagnetic relaxation enhancement (PRE) under high pressure to obtain distance restraints, and calculated the structure assisted by Bayesian inference. We conclude that the more disordered N_3 conformation observed at pH 4.0, 278 K, and 2.5 kbar largely retained the N_2 conformation, although the amide groups at residues 33–41 have more heterogeneous configurations and more contact with water, which differ from the native and N_2 states. The PRE-assisted strategy has the potential to improve structural characterization of proteins that lack NMR signals, especially for relatively more open and hydrated protein conformations.

Introduction

Proteins exist in a dynamic equilibrium among multiple conformations, which have marginal differences in Gibbs free energies[1,2]. High-energy, typically low-population protein states, i.e., open conformations of enzymes and locally disordered conformations, can be functionally important and/or at risk of forming toxic aggregates[3-5]. For instance, high-energy conformations have been identified in *Escherichia coli* dihydrofolate reductase, which mediate substrate and cofactor exchange[3], while transient structural distortion of superoxide dismutase 1 (SOD1) triggers aberrant oligomerization, and the misfolding and oligomerization of SOD1 have been linked to amyotrophic lateral sclerosis (ALS)[4].

We have focused on the structural characterization of the high-energy conformations of proteins using high-pressure NMR spectroscopy[6-9]. Elevated pressure can shift a population of protein conformers from the basic folded conformer to a fully unfolded conformer because the former has a larger partial molar volume[10]. Although solution NMR, including high-pressure NMR, is a useful technique to elucidate the dynamic equilibrium of proteins, structural determination remains difficult since conformational heterogeneity and the microsecond-to-millisecond time scale motions of the polypeptide chain lead to peak broadening and missing peaks in the NMR spectra[10,11]. In general, missing NMR signals result in a lack of structural information such as distance restraints derived from the nuclear Overhauser effect (NOE). To overcome this limitation, several NMR approaches that can provide structural restraints have been reported; for instance, paramagnetic relaxation enhancement (PRE)[12,13], which provides relatively longer distance restraints (e.g., ~25 Å) than the NOE (e.g., ~6 Å), and residual dipolar coupling (RDC),[14,15] which provides orientation restraints rather than distance restraints. However, to obtain the information, NMR signals must be observed in the NMR spectra. Therefore, it is still difficult to obtain structural information of regions with missing signals by conventional approaches.

Ubiquitin is a functionally important protein for many cellular activities, and thus its three-dimensional structure and conformational fluctuations have been extensively studied using biophysical approaches[14,16-20]. However, the structural details of the transient high-energy conformations of ubiquitin, e.g., folding-intermediate and partially unfolded conformations[19,21-23], are severely limited because of their low population. They are nevertheless of considerable interest, because local minima in the energy landscape are usually functionally important[9]. We previously reported that an alternatively folded conformation (N_2) accounted for ~20% of the population of wild-type ubiquitin at ambient pressure (298 K and pH 7.2), but ~70% of the population of the

ubiquitin Q41N variant (hereafter referred to as Q41N) at ambient pressure, and accounted for 97% of the population at 2500 bar (298 K and pH 7.2)[24]. Because there were only a couple of missing signals in N_2, we were able to determine the NOE-based structure of the conformation using high-pressure NMR[6,7].

More extreme solution conditions (low pH, high pressure and/or low temperature) increase the population of another state, here denoted N_3. This state resembles N_2, but is more disordered, specifically at residues 33-42, for which many of the amide signals are broadened or missing, and at the C-terminus. We showed that this state (pH 4.5 and 273 K) shares structural features with a proline-trapped kinetic intermediate based on pulse-labeling $^1H/^2H$-exchange NMR[11,23] It also has some features in common with an on-pathway folding intermediate of a ubiquitin variant (V17A/V26A) studied by Charlier et al[25] using pressure-jump NMR, which has a large chemical shift difference for the C-terminal residues between the native and folded intermediate states. The state N_3 is thus native-like, but is equally clearly an unfolding intermediate. The missing amide NMR signals of residues within the region 33–42 in N_3 prevented its NOE-based structural determination.

Here, we have used a low-pH and low-temperature (i.e., pH 4.0 and 278 K) condition, and show that N_3 has a more hydrated and denatured conformation than N_2, and thus moves further toward a denatured state. Moreover, we successfully determined the structure of N_3 using ubiquitin mutant Q41N with a simple strategy based on PRE-assisted NMR at high pressure.

Results and Discussion

NMR spectral changes under high pressure

We performed $^1H/^{15}N$ and $^1H/^{13}C$ HSQC measurements at a ^1H frequency of 800.34 MHz (AVANCE3-800) using a pressure-resistant NMR cell. HSQC cross-peaks of Q41N at pH 4.0, 278 K, and 1 bar were assigned to individual amino acid residues based on temperature and pH titration experiments, referring to assignments of Q41N at pH 7.2, 298 K, and 1 bar (BMRB: 11505)[24]. These specific low-pH and low-temperature conditions were chosen after consideration of protein stability and spectral quality.

Figure 1A shows the $^1H/^{15}N$ HSQC spectra of uniformly ^{15}N-labeled Q41N at pH 4.0 and 278 K recorded at 500-bar intervals between 1 bar and 2500 bar. These spectral changes were found to be reversible up to 2500 bar. Many cross-peaks showed substantial changes in ^1H and ^{15}N chemical shifts with increasing pressure. In general, chemical shifts are sensitive parameters for monitoring the structural changes of proteins. Specifically, changes in the chemical shifts of amide ^1H and ^{15}N are correlated to changes

in the strengths of hydrogen bonds as well as the backbone ϕ and ψ torsion angles[9], accompanied by mechanical compression and/or a transition into a different conformational state with a different compressibility. In order to observe these structural changes by changes in chemical shifts, the time scale of the structural changes should be much faster than the NMR chemical shift timescale (i.e., approximately in the millisecond range). Figure S1 shows pressure-induced chemical shifts of V70. We have previously shown that the N_2 conformation accounts for approximately 70% of the population of the ubiquitin Q41N variant at ambient pressure and 97% of the population at 2500 bar (298 K and pH 7.2), based on pressure-induced sigmoid-shaped chemical shifts[24]. The non-linear shifts in the present data indicate a similar increase in N_2 conformation under high pressure. N_2 is 65% populated at 1 bar, but 98% populated at 2500 bar (278 K and pH 4.0) according to the sigmoid-shaped analysis (see Methods in Supporting Information).

Pressure-induced changes in the intensities (i.e. volumes) of the cross-peaks present in the 1-bar spectrum (hereafter referred to as the original cross-peaks) are plotted in Figure 1B for Q41N. As the pressure increased, the cross-peak intensities of residues 28, 33, 36, and 39–41 preferentially decreased while the remaining peaks decreased more gradually. Quite similar results were observed for wild-type ubiquitin at pH 4.5 and 273 K but at much higher pressures, i.e., ~2500–3500 bar[11]. Because the intensities of the cross-peaks were restored at 298 K[26], we hypothesized that the loss of the $^{1}H/^{15}N$ HSQC signals is likely due to increased relaxation originating from conformational fluctuations and changes in solvation operating on the microsecond-to-millisecond time scale. In addition, new cross-peaks, corresponding to a disordered polypeptide chain, gradually appeared in the central part of the spectra recorded at pressures at and above 1500 bar. Figure 1C shows the pressure-induced incremental appearance of these new cross-peaks. Assignments for the new cross-peaks were obtained for uniformly $^{13}C/^{15}N$-doubly labeled Q41N at 278 K and 2500 bar using triple-resonance NMR experiments, i.e., CBCA(CO)NH, HNCACB, HNCA, HN(CO)CA, HNCO, and HN(CA)CO, on a DRX-600 (^{1}H, 600.23 MHz) spectrometer (Figure 1D). All new cross-peaks, including those for residues 28, 33, 36, and 39–41, cooperatively increased their intensities with increasing pressure, indicating a growing population of the entirely disordered conformation of the protein. In contrast to the pressure-induced loss of folded structure, which clearly occurred at different rates in different regions of the protein (Figure 1B), unfolded signals appeared at the same rate for the entire protein (Figure 1C).

To investigate the effects of pressure on the CH, CH_2, and CH_3 groups of Q41N, $^{1}H/^{13}C$ HSQC spectra were recorded at 500-bar intervals between 1 bar and 2500 bar at 278 K. As shown in Figure S2A in the Supporting Material, ^{1}H and ^{13}C chemical shifts of

several CH, CH_2, and CH_3 groups (e.g., K6Cβ, T9CβH, L43βH, I61CγH, E64CαH) changed significantly as the pressure increased. We note in particular the ring-current shifted signal from I61Hγ, which becomes even more strongly shifted with an increase in pressure, indicating a compression of the hydrophobic core. These changes were almost linear with pressure, indicating that the local structural or dynamic changes responsible for the linear shifts were constant over the pressure range studied[27]. Therefore, the structural change of N_1 to N_2 to N_3 is occurring within the same folded ensemble. Figures 2A and 2B show plots of the cross-peak intensities of the CαH and CβH groups, respectively, at different pressures relative to those observed at 1 bar. Many of these signals gradually lost their intensities with increasing pressure. Figure S2B shows the HSQC spectra of the CαH groups at 1 bar and 2500 bar. Figure S2C shows the pressure-induced incremental appearance of some well-isolated new cross-peaks of the CαH groups (depicted by green arrows in Fig. S2B). New cross-peaks, corresponding to a disordered polypeptide chain, gradually appeared in the spectra recorded at pressures at and above 1500 bar, similar to the data of the amide groups (Fig. 1C). These results also indicate a growing population of completely disordered conformation of the protein. However, the CβH groups of residues 23, 31, and 40 showed preferential decrease in their intensities, similar to the data of the backbone amide groups.

Pressure-induced changes in the cross-peak intensities of the NH, CαH, and CβH groups are summarized for each residue in Figure S3. Most of these signals lose their intensities with the same pressure dependence, except some of the amide group signals (i.e., residues 28, 33, 36, and 39–41) and the CβH group signals of residues 23, 31, and 40, showing initiation of global unfolding above 1500 bar, but with localized differences in unfolding, specifically formation of the partially unfolded intermediate state N_3.

Pressure-induced broadening and disappearance of NMR signals

To further examine the pressure-induced changes in the backbone dynamics of Q41N, we performed ^{15}N-transverse relaxation experiments at elevated pressure using a DRX-600 (^{1}H, 600.23 MHz) spectrometer. ^{15}N-transverse relaxation of individual amide groups is affected by chemical exchange processes taking place at the microsecond-to-millisecond time scale as well as internal motions at the picosecond-to-nanosecond timescale. Figure 3 shows the ^{15}N-transverse relaxation rate constants, R_2, estimated for the original cross-peaks. Larger R_2 values than average were clearly observed for residues 16, 23, 25, 33, 39, and 70-71 at 1 bar, indicating the presence of chemical exchange processes[6,29,30]. Note that cross-peaks of E24 and G53 were missing in the spectrum obtained under the experimental solution condition. Specifically, a backbone flip motion of E51-R54

coupled with a deformation of the hydrogen bond between I23H^N-R54CO and a side-chain rearrangement of Ile23 affect R_2 values of residues 23–25 and 53[29,30]. In addition, reorientation of the C-terminus of α_1-helix and β_5-strand coupled with the N_1-N_2 conformational transition affects the R_2 value of residues 70-71[6,7].

With increasing pressure up to 2500 bar, remarkable increases in the R_2 values were observed specifically for the amide groups of residues 28–39. This can be explained by an increasing contribution of chemical exchange processes (i.e., R_{ex}) to the R_2 at elevated pressures. The N_2 conformation accounts for approximately 70% of the population of the ubiquitin Q41N variant at ambient pressure, and the population of N_2 increases with increasing pressure (Fig. S1). Therefore, N_2 is more highly populated at higher pressures, resulting in a sharp decline in the contribution to R_{ex} from the N_1-N_2 exchange. Although the N_1-N_2 exchange rate constant is likely to decrease with increasing pressure as shown in WT (i.e., 4.8×10^5 s^{-1} at 30 bar, 1.7×10^5 s^{-1} at 3 kbar, pH 4.6 and 293 K)[6], the contribution of the population shift to R_{ex} will dominate that of the rate constants and reduce R_{ex} rates arising from the N_1-N_2 exchange. We therefore conclude that the increases seen in R_2 in the 28-39 region at high pressure are due an increased population of the locally disordered conformation N_3.

Under the lower pH and lower temperature condition (i.e., pH 4.0, 278 K, and 2500 bar), Q41N is expected to exhibit greater destabilization of the hydrogen bonds in the backbone and partial exposure of amide groups to the solvent. Indeed, pressure-induced increments of water–amide proton interactions were detected spatially at the C-terminal side of wild-type ubiquitin (e.g., residues 32–35, 40–41, and 71) at pH 7.4 and 298 K by CLEANEX-PM NMR experiments[31]. We therefore attempted to measure water-amide proton exchange in our low pH/low temperature conditions, to determine whether signal loss could be due to solvent exchange. Rate constants of water–amide proton exchange were too small to detect using CLEANEX-PM experiments under acidic conditions (pH 4.0). Indeed, no signals were observed using the CLEANEX-PM experiments with a 100-ms mixing time at 1 and 2500 bar (data not shown). According to a 1-millisecond molecular dynamics simulation for BPTI, two water molecules must be directly coordinated to backbone amides in an open state, to allow amide protons to exchange with water[32]. Therefore, the pressure-induced broadening and loss of cross-peak intensities of the amide and CβH groups (Fig. 1A and Fig. 2B) in the regions from the α_1-helix to the β_3-strand are concluded to originate from heterogeneity of atomic packing, including protein and hydration water, and/or fluctuation among the conformations within the NMR chemical shift timescale (i.e., the millisecond scale).

In contrast to pressure-induced increments of R_2, a decline of R_2 was observed

for E16 (Fig. 2) of the Q41N variant unlike WT. Actually, the value of E16 was significantly larger than that of WT at 1 bar[24], indicating that the substitution of Q41 to N41 increased the local dynamics or conformational heterogeneity at the opposite side of the protein, namely at and around E16. The decline of R_2 implies that pressure reduced the effects of the substitution, although the cause is still unknown.

PRE-assisted NMR structure determination at high pressure

When the NMR spectral quality is poor due to peak broadening and missing peaks, it is often difficult to obtain a sufficient number of distance restraints for protein structural determination. A series of triple- and double-resonance NMR experiments for signal assignments were performed on uniformly $^{13}C/^{15}N$-doubly labeled Q41N using a DRX-600 spectrometer at pH 4.0, 278 K and 2500 bar (see Methods). Using an AVANCE3-800 spectrometer, we simultaneously acquired the $^{13}C/^{15}N$-edited NOESY spectrum for uniformly $^{13}C/^{15}N$-doubly labeled Q41N at pH 4.0, 278 K, and 2500 bar to collect NOE data. Barely any inter-residue NOEs were observed between residues 35–41 and the rest of the protein (Fig. S4A). Structural calculation of Q41N was performed with CYANA version 3.97 using 1238 NOE-based distance restraints and 74 torsion-angle restraints derived using TALOS+[33] (Fig. S5A). Details of the restraints and geometrical statistics are shown in Table S2. However, structural convergence was rather poor between the end of the α_1-helix and the β_3-strand region as well as in the β_5-strand at the C-terminus. The root-mean-square-deviation (RMSD) to the mean coordinates for the backbone atoms of residues 1–70 was 0.55 Å.

To overcome the limitation of the low number of distance restraints between the NMR-invisible amide groups and -visible sites on the convergence of the ensemble, we performed PRE-assisted structure determination. PRE effects from the paramagnetic agent *S*-[(1-oxyl-2,2,5,5-tetramethyl-2,5-dihydro-1h-pyrrol-3-yl)methyl] methanesulfonothioate (MTSL) tagged in the loop region where pressure-induced broadening and NMR signal disappearance occurred were observed on NMR-visible amide groups. Cysteine residues are usually used to add MTSL. To minimize the effects of residue-substitution to cysteine on protein stability and dynamics, we chose to label K33 and Q40, which are exposed to the solvent. E34, I36, P37, and P38 were excluded as candidates for the substitution because the side-chains of E34 and I36 face the inside of the protein and thus the residue-substitution and -modification may significantly change the stability and dynamics of the region. A *cis-trans* isomerization of P37 and/or P38 is related to a population of the cis-trapped kinetic intermediate[23] and thus the substitution may change structural properties of the equilibrium intermediate. Ubiquitin

G35C/Q41N variant was not sufficiently produced by the current *E. coli* expression (see Methods). Note that wild-type ubiquitin has no cysteine residues. We therefore prepared uniformly ^{15}N-labeled ubiquitin K33C/Q41N and Q40C/Q41N double variants. When the spin-labeled (oxidized) MTSL was covalently bound to the substituted cysteine sidechain, the protein possesses a paramagnetic property resulting from an unpaired electron present in MTSL. The paramagnetic effects from the unpaired electron are very strong, which affect the spin-relaxation of nuclei up to an approximate 25-Å distance. When the spin-label is reduced with 2-fold excess ascorbic acid, the protein becomes diamagnetic. ^{1}H/^{15}N HSQC spectra of ubiquitin K33C/Q41N and ubiquitin Q40C/Q41N were measured with the oxidized and reduced forms of MTSL at pH 4.0, 278 K, and 2500 bar using a DRX-600 spectrometer. HSQC cross-peaks in the double variant proteins were assigned to individual amino acid residues using ^{15}N-edited TOCSY and NOESY experiments based on assignments of ubiquitin Q41N.

Effects of residue-substitution and MTSL-tag were evaluated in terms of structure and dynamics of the protein. At 1 bar, chemical shift changes (i.e. $[(\Delta\delta\,\mathrm{H})^2 + (\Delta\delta\,\mathrm{N}/5)^2]^{0.5}$) of greater than 0.2 ppm were observed at residues 40, 43–44, and 71 in the MTSL-tagged K33C/Q41N variant (Fig. S6A) and at residues 45 and 72–74 in the MTSL-tagged Q40N/Q41N variant (Fig. S6B). At 2500 bar, changes in chemical shift were smaller particularly at residues 42-44. Because large chemical shift changes (e.g. greater than 0.2 ppm) were observed only at residues 71-73 spatially proximal to the substituted residue at 2500 bar, the effects of residue-substitution and MTSL-tag on the average conformation of the intermediate are presumed to be limited to the C-terminal strand. The effects on the backbone dynamics were evaluated by analysis of line-broadening (Figs. S6A and S7A) and ^{15}N spin-relaxation (Fig. S8). In the case of the MTSL-tagged K33C/Q41N variant, more cross-peaks of residues 27-42 disappeared from the spectrum (Figs. S6A and S7A), while results of the MTSL-tagged Q40C/Q41N variant are almost identical to the Q41N variant (Figs. S6B and S7B). In addition, a similar decline in the cross-peak volumes of residues 33, 39 and 41 was observed in the MTSL (reduced form)-tagged Q40C/Q41N variant with increasing pressure (Fig. S8), indicating that the MTSL-tagged variant also shares similar disordered conformation with that of Q41N and WT. The missing signals with the addition of the MTSL-tag prevented the same analysis of the K33C/Q41N variant. We also compared the rotational correlation time, τ_r, derived from ^{15}N-T_1/T_2 of each backbone amide group at 2500 bar and 278 K with assuming no anisotropy of motion, among the variants (Fig. S8). τ_r values were not altered by the residue-substitution and modification. Taken together, the effects of the residue-substitution and MTSL-tag on the protein conformation are limited, although backbone

dynamics of the regions specifically from the α_1-helix to the β_3-strand seems to be sensitive to residue-substitution and -modification as well as pressure perturbation. Thus, it is meaningful to supply additional distance information between the partially disordered region (i.e., α_1-helix to the β_3-strand) and other sites using the paramagnetic tag. As discussed below, PRE-based distance information was used as gentle distance restraints for structure determination (see Methods) to reduce the risk of overfitting the structural models. Moreover, PRE-based distance restraints for residues 71-76, whose chemical shifts are sensitive to residue-substitution and -modification, were not used for structural determination.

Rather than directly measuring the relaxation rates from a series of two-dimensional NMR experiments, relaxation rates can be indirectly obtained from the ratios of the peak heights of a paramagnetic sample to those of a diamagnetic sample, i.e., I_{para}/I_{dia}[34]. Figures 4A and 4B show the residue-specific I_{para}/I_{dia} ratios for ubiquitin K33C/Q41N and ubiquitin Q40C/Q41N, respectively, measured at 1 bar and 2500 bar. A lower I_{para}/I_{dia} value indicates a greater PRE effect. At 1 bar, the ratios were almost null for the residues spatially close to the spin-labeled MTSL (i.e. residues 7–17, 30–43, and 69–72 in ubiquitin K33C/Q41N; residues 7–11, 35–43, 52–53, and 69–76 in ubiquitin Q40C/Q41N). At 2500 bar, the I_{para}/I_{dia} ratio showed both increases and decreases in value for several sites. For instance, increases in the ratio for residues 5–6 and 11–12 in ubiquitin Q40C/Q41N indicated that the PRE effects were weakened, and thus the residues moved away from residue 40. Decreases in the ratio for residues 25–29, 49–51, and 54–55 in ubiquitin Q40C/Q41N indicated that these residues are located closer to residue 40. Note that pressure-induced changes in the orientation of the MTSL side chain may also affect changes in the I_{para}/I_{dia} ratio. Based on the results of the PRE experiments, a total of 140 PRE-based distance restraints were used for the structural determination of Q41N at 2500 bar. Intensity ratios were converted into distances according to a previously described method[34] (see Methods). Figure S5B shows 20 structural models calculated with 140 PRE- and 1246 NOE-based distance restraints, and 74 torsion angle restraints. The number of inter-residue NOEs for each residue is shown in Figure S4B. Note that a consequence of addition of the PRE-based restraints is that the total number of NOEs accepted in the automated NOE assignments by CYANA is slightly increased. In particular, the number of inter-residue NOEs was increased for residues 40 and 41. The RMSD for the backbone atoms of residues 1–70 decreased from 0.55 Å to 0.45 Å, and the improvement of structural convergence was particularly noticeable at residues 33–41 (Fig. S5).

The line-broadening observed for residues 33-41 implies exchange between

multiple conformations in this region. The structures calculated therefore represent r^{-6}-weighted averages. It is worth noting that this statement is true for all NMR structures obtained using NOE distance restraints: the difference here is that we can be confident that there is conformational exchange occurring, and it is slower (and therefore possibly more extensive) than normal.

NMR structure refinement based on Bayesian inference

We used an NMR structure refinement method based on Bayesian inference[35] implemented in CYANA[36]. The method involves a molecular dynamics simulation to quickly obtain global structures with automatic NOE assignment and subsequent structure refinement by Bayesian inference, providing a useful method when only sparse experimental data are available. Figures 5A and 5B show the Bayesian-refined structures determined without and with PRE-based distance restraints, respectively. A total of 1900 structures are presented in each top panel. Principal components analysis (PCA) was performed for the Cα position of residues 1–70 to visualize the distributions of the calculated structural ensembles. The bottom panels show the first and second principal components, PC1 and PC2, in the PCA. Without PRE restraints, the 1900 structures were widely distributed into three main regions in the PC1-PC2 map, which is likely attributed to the limited distance restraints between the NMR-visible and -invisible regions. In contrast, the structures were more tightly grouped in the map with PRE restraints included in the Bayesian-refined structure calculation. Twenty of the lower energy structures from the 1900 models were selected, showing an RMSD for residues 1–70 of the PRE-assisted and Bayesian-refined structures of 0.27 Å for backbone atoms and 0.48 Å for heavy atoms, representing a remarkable improvement of structural convergence. The correlation between the distance calculated from the PRE and the distances determined from 20 structural models calculated with PRE or without PRE is shown in Figure S8. When PRE data were used in the structural calculation, the correlation was generally improved and most expected distances determined from three-dimensional structures appeared within 5 Å boundaries.

Pressure-induced unfolding of ubiquitin

Comparing the Bayesian-refined structure of Q41N at pH 4.0, 278 K, and 2500 bar (N_3) with the wild-type conformation (i.e., N_1 conformation, PDB: 1D3Z), a greater than 2.0-Å deviation of the Cα atom position was only observed at residues 8-10, 35, 38–40, and above 70 (Fig. S10), indicating reorientation of the loop region and the C-terminal β5-

strand, resulting in a more open conformation at the C-terminal side of the protein. This phenomenon is similar to the structural characteristics of the protein observed at pH 7.2, 298 K, and 2500 bar, indicating that the protein under these solution conditions largely retained the N_2 conformation, the main difference being that the amide groups at residues 33–41 seemed to have more heterogeneous configurations and more contact with water. Indeed, deviation in the Cα atom position between the N_3 structure (pH 4.0, 278 K, and 2500 bar) and N_2 conformation (pH 7.2 and 298 K, and 2500 bar, PDB: 2RU6) was small (Fig. S10). According to the kinetic NMR experiments, the intermediately folded species was trapped with a cis conformer of P37 and/or P38 peptide bonds. However, the P37 and P38 peptide bonds entirely adopted trans conformations in the equilibrium N_3 structure. The ψ torsion angles were closely similar to those of N_2, specifically those of P37 and P38 (PDB: 6K4I). In addition, pressure-induced changes in chemical shifts (e.g., ^{1}H and ^{13}C) and cross-peak volumes of P37 and P38 were not unusual, and inter-residue NOEs were also consistent with the trans conformation of P37 and/or P38 peptide bonds (Figs. S3 and S11). In other words, we can characterize four states whose populations can be controlled using temperature, pH and pressure: $N_1 \leftrightarrow N_2 \leftrightarrow N_3 \leftrightarrow U$, plus a further kinetically trapped cis-proline conformation.

Overall, the more disordered conformation N_3 observed at pH 4.0, 278 K, and 2500 bar represents a further unravelling at the same 33–41 region, that differs between N_1 and N_2. Based on hydrogen/deuterium exchange NMR experiments, Englander and coworkers have suggested the presence of cooperative unfolding units in protein structures [37]. Residues 33–41, which are involved in the conformational transition from N_1 to N_2 and then have more heterogeneous configurations and more contact with water in N_3, could be the primary cooperative unfolding unit of ubiquitin.

Conclusions

We demonstrated that the Q41N variant of ubiquitin, like the WT, shows pressure-induced loss of backbone amide group signals at several residues in the 33–41 region, while most of the CαH and CβH groups showed no preferential decline in cross-peak intensities, showing more heterogeneous configurations and more contact with water at those backbone amide sites under high pressures. Because residues 33–41 are also involved in the N_1-N_2 transition, they could be the primary cooperative unfolding unit of the protein. In addition, we have observed PRE under high pressures for the first time, and by adopting PRE-based distance restraints, we determined the structure of the N_3 conformation of ubiquitin. Peak-broadening and missing peaks resulting from

conformational exchange on the microsecond-to-millisecond time scale often reduce the quality of NMR spectra, making NOE-based structural determination difficult. The PRE-assisted strategy has the potential to improve structural characterization of proteins that have missing NMR signals, especially for relatively more open and hydrated protein conformations.

Methods

Sample preparation. Uniformly ^{15}N-labeled and ^{13}C/^{15}N-doubly labeled Q41N ubiquitin and uniformly ^{15}N-labeled double-variant ubiquitin K33C/Q41N or Q40C/Q41N were produced by conventional *Escherichia coli* expression (e.g. pGEX-6P-1 vector and *E. coli* competent cells BL21 (DE3))[24]. The cysteine variants were dissolved in 30 mM D-acetate buffer at pH 4.0, mixed with MTSL (Toronto Research Chemicals, Ontario, Canada), and incubated for approximately 12 h at 277 K. The protein solution was filtered and concentrated using Microcon (Merck Millipore, Burlington, MA, USA). The final protein solution was adjusted to a concentration of 0.3 mM for PRE experiments and to 1.0 mM for NOESY experiments in 30 mM D-acetate buffer (pH 4.0) containing 12% $^{2}H_2O$. The spin-labeled MTSL was reduced with 2-fold excess ascorbic acid relative to the protein concentration.

NMR measurements and analyses. NMR experiments were performed on an AVANCE3-800 (^{1}H, 800.34 MHz) or DRX-600 (^{1}H, 600.23 MHz) spectrometer (Bruker, Coventry, UK and Bruker, Billerica, MA, USA, respectively) using a pressure-resistant NMR cell (Daedalus Innovations, Aston, PA, USA) and a TXI probe (Bruker, Coventry, UK and Bruker, Billerica, MA, USA, respectively). Triple- and double-resonance NMR experiments, i.e., CBCA(CO)NH, HNCACB, HNCA, HN(CO)CA, HNCO, HN(CA)CO, HBHA(CO)NH, HCC(CO)NH, CC(CO)NH, HCCH-TOCSY, CCH-TOCSY, and ^{15}N edited TOCSY-HSQC for signal assignments were performed on uniformly ^{13}C/^{15}N-doubly labeled Q41N using a DRX-600 spectrometer at 278 K and 2500 bar. ^{1}H/^{15}N HSQC, ^{1}H/^{13}C HSQC, and simultaneous ^{13}C/^{15}N-edited NOESY spectra were recorded on uniformly ^{13}C/^{15}N-doubly labeled Q41N using an AVANCE3-800 spectrometer, while ^{15}N-longitudinal and transverse relaxation experiments were recorded on uniformly ^{15}N-labeled Q41N using a DRX-600 spectrometer. ^{1}H/^{15}N HSQC and ^{1}H/^{13}C HSQC spectra at different pressure were collected with a delay of 1 second. The simultaneous ^{13}C/^{15}N-edited NOESY consisting of 308 complex t_1 points, 64 complex t_2 points, and 2048 real t_3 points used a 100 ms mixing time. The spectral widths were 13.95 ppm (^{1}H, F_1), 26.0

ppm/23.0 ppm (^{15}N/^{13}C, F_2), and 13.95 ppm (^{1}H, F_3). A 256 complex × 2048 real data matrix was acquired for 10 different T_1 delays: 10, 20, 40, 70, 100s, 200, 400, 600, 900, and 1200 ms. A CPMG type pulse sequence was used to measure ^{15}N transverse relaxation time constants, T_2. A 256 complex × 2048 real data matrix was acquired for 10 different T_2 delays: 20, 35, 50, 70, 100, 130, 160, 200, 250, and 280 ms. For the ^{15}N- T_1 and T_2 experiments, the spectral widths were 29.0 ppm (^{15}N, F_1) and 14.56 ppm (^{1}H, F_2). Schemes for the ^{15}N-T_1 and -T_2 experiments are described in the literature[38]. To measure PRE, ^{1}H/^{15}N HSQC spectra of the MTSL-bound ubiquitin K33C/Q41N and Q40C/Q41N were collected for the oxidized and reduced forms of MTSL at 278 K and 1 bar or 2500 bar using a DRX-600 spectrometer. A 128 complex × 2048 real data matrix was acquired with spectral widths 29.0 ppm (^{15}N, F_1) and 14.56 ppm (^{1}H, F_2). NMR data were processed using Topspin version 3.2 (Bruker, Billerica, MA, USA), NMRPipe[39], NMRViewJ[40], and KUJIRA[41]. The signal assignments of Q41N at pH 7.2, 298 K, and 2500 bar (BMRB: 11505) were used as reference. Temperature and pH titration experiments were performed to obtain resonance assignments of Q41N at pH 4.0, 278 K, and 2500 bar.

The ratio of the peak heights of a paramagnetic sample to those of a diamagnetic sample, i.e., I_{para}/I_{dia} is equal to

$$\frac{I_{para}}{I_{dia}} = \frac{R_{2int}\exp(-R_{2PRE}t)}{R_{2int}+R_{2PRE}} \quad (1)$$

where R_{2int} and R_{2PRE} are the intrinsic transverse relaxation rate and the PRE effects on transverse relaxation rate, respectively, for each amide proton, and t is the total INEPT evolution time of the HSQC (11.5 ms). The R_{2int} for each amide proton was estimated from the half-height line-widths of peaks of the diamagnetic sample. The I_{para}/I_{dia} was used to estimate R_{2PRE}. The R_{2PRE} was converted into distance using the following equation,

$$r = \left[\frac{K}{R_{2PRE}}\left(4\tau_c + \frac{3\tau_c}{1+\varpi_H^2\tau_c^2}\right)\right]^{1/6} \quad (2)$$

where r is the distance between the unpaired electron and nucleus, ω_H is the Larmor frequency of proton, K is 1.23×10^{-32} cm^6 s^{-2}, and τ_c is the correlation time given as $1/\tau_c = 1/\tau_r + 1/\tau_e$ (τ_r the rotational correlation time of the electron-nucleus vector, τ_e the electron spin relaxation time)[34]. Because τ_e (>10^{-7} s) of the unpaired electron is much longer than τ_r, τ_c equals approximately τ_r. τ_c ($\approx \tau_r$) was estimated assuming no anisotropy of motion using the equation:

$$\tau_c \approx \tau_r = (1/2\omega_N)\sqrt{(6\,T_1/T_2 - 7)} \quad (3)$$

where ω_N is the ^{15}N frequency in radians s^{-1} [42]. In the case of Q41N ubiquitin at the current conditions (i.e. 278 K and 2500 bar), τ_r values were distributed within 5~20 ns, and the mean of τ_r in the secondary-structured regions was 8.4 ns. The half-height line-widths ($\Delta\nu$(hertz) = R_{2int}/π) were 15~35 Hz for ^1H, and the mean was 20 Hz. Estimated distances from the I_{para}/I_{dia} with different τ_r and R_{2int} are plotted in Fig. S12. In the current case, taking into account the diverse values of τ_r and R_{2int} and the uncertainty of the MTSL position due to the side-chain flexibility, three classes of distance restraints between CβH of K33 (or Q40) and other amide protons were used for structure calculations as described below.

Structure calculations for the $^{13}C/^{15}N$-doubly labeled Q41N were performed with CYANA ver. 3.97. Automated NOE peak assignments were performed by the CYANA program. Technical details and reliability of the program are discussed in the literature[37]. Distance restraints were obtained from a simultaneous acquisition $^{13}C/^{15}N$-edited NOESY spectrum with a 100 ms mixing time. Backbone ϕ and ψ angle restraints were derived using TALOS+[33]: $-120° < \phi < -20°$ and $-100° < \psi < 0°$ for an α-helix, and $-200° < \phi < -80°$ and $40° < \psi < 220°$ for a β-sheet. Distance restraints were established based on the PRE experiments: if $I_{para}/I_{dia} < 0.15$ or $0.85 < I_{para}/I_{dia}$, it was assumed that the distance between the spin label and the nucleus was less than 14.6 Å or more than 18.1 Å, respectively. If $0.15 \leq I_{para}/I_{dia} \leq 0.85$, a distance restraint of 11.7 Å-23.1 Å was imposed (the lower limit at 0.15-the upper limit at 0.85) (Fig. S12).

We used the NMR structure refinement method based on Bayesian inference[34] implemented in CYANA ver. 3.97[36]. The twenty lowest energy structures from the 1900 models were selected, and energy minimization was performed with distance and angle restraints using OPALp[43]. In order to support the validity of this approach, the distance calculated from the PRE and distances determined from 20 structural models were compared.

References

1 Bai YW, Milne JS, Mayne L. & Englander SW (1994) Protein stability parameters measured by hydrogen-exchange. Proteins-Structure Function and Genetics 20: 4-14.

2 Li R, Woodward C (1999) The hydrogen exchange core and protein folding. Protein Sci 8: 1571-1590.

3 Boehr DD, McElheny D, Dyson HJ, Wright PE (2006) The dynamic energy landscape of dihydrofolate reductase catalysis. Science 313: 1638-1642.

4 Teilum K, Smith MH, Schulz E, Christensen LC, Solomentsev G, Oliveberg M, Akke M (2009) Transient structural distortion of metal-free Cu/Zn superoxide dismutase triggers aberrant oligomerization. Proc Natl Acad Sci USA 106: 18273-18278.

5 Mulder FAA, Mittermaier A, Hon B, Dahlquist FW, Kay LE (2001) Studying excited states of proteins by NMR spectroscopy. Nat Struct Biol 8: 932-935.

6 Kitahara R, Yokoyama, S, Akasaka (2005) NMR snapshots of a fluctuating protein structure: ubiquitin at 30 bar-3 kbar. J Mol Biol 347: 277-285.

7 Kitazawa S, Kameda T, Kumo A, Yagi-Utsumi M, Baxter NJ, Kato K, Williamson MP, Kitahara R (2014) Close identity between alternatively folded state N_2 of ubiquitin and the conformation of the protein bound to the ubiquitin-activating enzyme. Biochemistry 53:447-449.

8 Baxter NJ, Zacharchenko T, Barsukov IL, Williamson MP (2017) Pressure-dependent chemical shifts in the R3 domain of talin show that it is thermodynamically poised for binding to either vinculin or RIAM. Structure 25:1856-1866.

9 Williamson MP, Kitahara R (2019) Characterization of low-lying excited states of proteins by high-pressure NMR. Biochim Biophys Acta Proteins Proteom 1867: 350-358.

10 Kitahara R, Yamada H, Akasaka K, Wright PE (2002) High pressure NMR reveals that apomyoglobin is an equilibrium mixture from the native to the unfolded. J Mol Biol 320:311-319.

11 Kitahara R, Akasaka K (2003) Close identity of a pressure-stabilized intermediate with a kinetic intermediate in protein folding. Proc Natl Acad Sci USA 100:3167-3172.

12 Clore GM, Iwahara J (2009) Theory, practice, and applications of paramagnetic relaxation enhancement for the characterization of transient low-population states of biological macromolecules and their complexes. Chem. Rev. 109:4108-4139.

13 Schwieters CD, Bermejo GA, Clore GM (2018) Xplor-NIH for molecular structure determination from NMR and other data sources. Protein science 27:26-40.

14 Tjandra N, Grzesiek S, Bax A (1996) Magnetic field dependence of nitrogen-proton J splittings in ^{15}N-enriched human ubiquitin resulting from relaxation interference and residual dipolar coupling. J Am Chem Soc 118:6264-6272.

15 Tjandra N, Bax A (1997) Direct measurement of distances and angles in biomolecules by NMR in a dilute liquid crystalline medium. Science 278:1697-1697.

16 Lange OF, Lakomek NA, Fares C, Schroder GF, Walter KF, Becker S, Meiler J, Grubmuller H, Griesinger C, de Groot BL (2008) Recognition dynamics up to microseconds revealed from an RDC-derived ubiquitin ensemble in solution. Science 320:1471-1475.

17 Tollinger M, Sivertsen AC, Meier BH, Ernst M, Schanda P (2012) Site-resolved measurement of microsecond-to-millisecond conformational exchange processes in proteins by solid-state NMR spectroscopy. J Am Chem Soc 134:14800-14807.

18 Lindorff-Larsen K, Best RB, DePristo MA, Dobson CM, Vendruscolo M (2005) Simultaneous determination of protein structure and dynamics. Nature 433:128-132.

19 Piana S, Lindorff-Larsen K, Shaw DE (2013) Atomic-level description of ubiquitin folding. Proc Natl Acad Sci USA 110: 5915-5920.

20 Nisius L, Grzesiek S (2012) Key stabilizing elements of protein structure identified through pressure and temperature perturbation of its hydrogen bond network. Nature Chem 4:711-717..

21 Charlier C, Alderson TR, Courtney JM, Ying JF, Anfinrud P, Bax A (2018) Study of protein folding under native conditions by rapidly switching the hydrostatic pressure inside an NMR sample cell. Proc Natl Acad Sci USA 115:E4169-E4178.

22 Charlier C, Courtney JM, Alderson TR, Anfinrud P, Bax A (2018) Monitoring ^{15}N chemical shifts during protein folding by pressure-jump NMR. J Am Chem Soc 140:8096-8099.

23 Briggs MS, Roder H (1992) Early hydrogen-bonding events in the folding reaction of ubiquitin. Proc Natl Acad Sci USA 89: 2017-2021.

24 Kitazawa S, Kameda T, Yagi-Utsumi M, Sugase K, Baxter NJ, Kato K, Williamson MP, Kitahara R (2013) Solution structure of the Q41N variant of ubiquitin as a model for the alternatively folded N_2 state of ubiquitin. Biochemistry 52:1874-1885.

25 Charlier C, Courtney JM, Anfinrud P, Bax A (2018) Interrupted pressure-jump NMR experiments reveal resonances of on-pathway protein folding intermediate. J Phys Chem B 122:11792-11799.

26 Kitahara R, Yamada H, Akasaka K (2001) Two folded conformers of ubiquitin revealed by high-pressure NMR. Biochemistry 40:13556-13563.

27 Kitahara R, Hata K, Li H, Williamson MP, Akasaka K (2013) Pressure-induced chemical shifts as probes for conformational fluctuations in proteins. Prog NMR Spec 71:35-58.

28 Kitahara R, Simorellis AK, Hata K, Maeno A, Yokoyama S, Koide S, Akasaka K (2012) A delicate interplay of structure, dynamics, and thermodynamics for function: a high pressure NMR study of outer surface protein A. Biophys J 102:916-926.

29 Salvi N, Ulzega S, Ferrage F, Bodenhausen G (2012) Time scales of slow motions in ubiquitin explored by heteronuclear double resonance. J Am Chem Soc 134:2481-2484.

30 Sidhu A, Surolia A, Robertson AD, Sundd M (2011) A hydrogen bond regulates slow motions in ubiquitin by modulating a beta-turn flip. J Mol Biol 411:1037-1048.

31 Kitazawa S, Aoshima Y, Wakamoto T, Kitahara R (2018) Water-protein interactions coupled with protein conformational transition. Biophys J 115:981-987.

32 Persson F, Halle B (2015) How amide hydrogens exchange in native proteins. Proc Natl Acad Sci USA 112: 10383-10388.

33 Shen Y, Delaglio F, Cornilescu G, Bax A (2009) TALOS+: a hybrid method for predicting protein backbone torsion angles from NMR chemical shifts. J Biol NMR 44:213-223.

34 Battiste JL, Wagner G (2000) Utilization of site-directed spin labeling and high-resolution heteronuclear nuclear magnetic resonance for global fold determination of large proteins with limited nuclear Overhauser effect data. Biochemistry 39:5355-5365.

35 Ikeya T, Ikeda S, Kigawa T, Ito Y, Güntert P (2016) Protein NMR structure refinement based on Bayesian inference. J. Phys. Conf. Ser. 699, doi:Artn 01200510.1088/1742-6596/699/1/012005.

36 Herrmann T, Güntert P, Wüthrich K (2002) Protein NMR structure determination with automated NOE assignment using the new software CANDID and the torsion angle dynamics algorithm DYANA. J Mol Biol 319:209-227.

37 Rumbley J, Hoang L, Mayne L, Englander SW (2001) An amino acid code for protein folding. Proc Natl Acad Sci USA 98:105-112.

38 Kay LE, Torchia D, Bax A (1989) Backbone dynamics of proteins as studied by ^{15}N inverse detected heteronuclear NMR spectroscopy: Application to Staphylococcal nuclease. Biochemistry 28: 8972-8979.

39 Delaglio F, Grzesiek S, Vuister GW, Zhu G, Pfeifer J, Bax A (1995) Nmrpipe - a multidimensional spectral processing system based on Unix pipes. J Biol NMR 6:277-293.

40 Johnson BA, Blevins RA (1994) Nmr View - a Computer program for the visualization and analysis of NMR data. J Biol NMR 4:603-614.

41 Kobayashi N, Iwahara J, Koshiba S, Tomizawa T, Tochio N, Güntert P, Kigawa T, Yokoyama S (2007) KUJIRA, a package of integrated modules for systematic and interactive analysis of NMR data directed to high-throughput NMR structure studies. J Biol NMR 39:31-52.

42 Anthis NJ, Clore GM (2000) The length of the calmodulin linker determines the extent of transient interdomain association and target affinity. J Am Chem Soc 135: 9648-9651.

43 Koradi R, Billeter M, Güntert P. (2000) Point-centered domain decomposition for parallel molecular dynamics simulation. Comput Phys Commun 124: 139-147.

44 Lovell SC, Davis IW, Arendall WB 3rd, de Bakker PI, Word JM, Prisant MG, Richardson JS, Richardson DC (2003) Structure validation by Cα geometry: ϕ, ψ and Cβ deviation. PROTEINS: Struct., Funct., Bioinforma 50: 437-450.

Figures

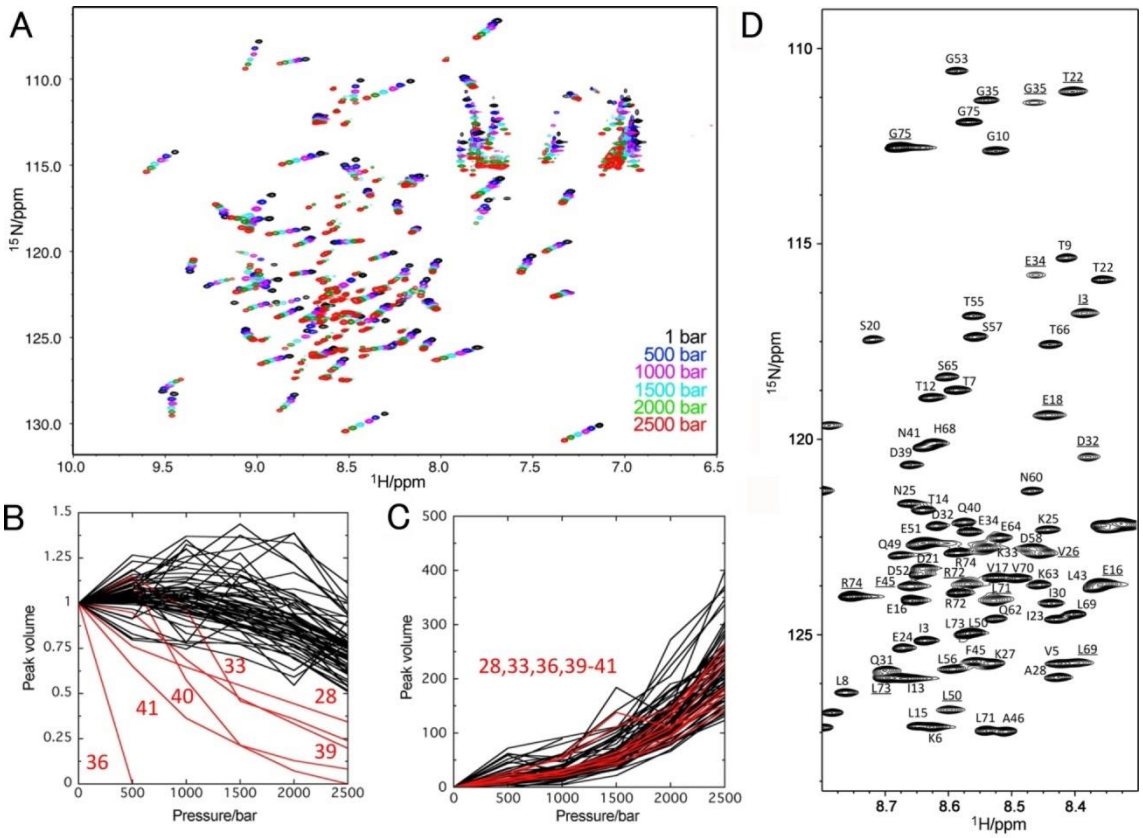

Figure 1. ^{1}H/^{15}N HSQC spectral analysis for backbone amide groups. (A) Overlay of ^{1}H/^{15}N HSQC spectra of uniformly ^{13}C/^{15}N-labeled ubiquitin Q41N at different pressures, from 1 bar to 2500 bar, at pH 4.0 and 278 K. (B) Volumes of original cross-peaks at different pressures relative to those at 1 bar (red, residues 28, 33, 36, 39–41; black, other residues). (C) Volumes of new cross-peaks at different pressures (red, residues 28, 33, 36, 39–41; black, other residues). Peak volumes are depicted in arbitrary units. (D) ^{1}H/^{15}N HSQC spectrum at 2500 bar and signal assignments. Assignments of the original cross-peaks are underlined and the others are new cross-peaks.

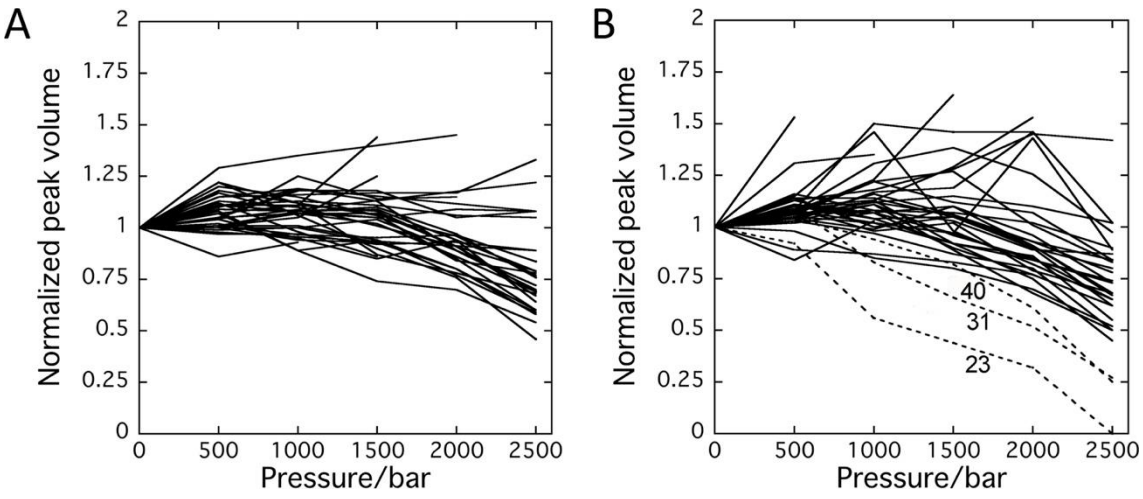

Figure 2. Changes in peak volumes of CH groups versus pressure. Peak volumes of the (A) CαH and (B) CβH groups of uniformly $^{13}C/^{15}N$-labeled ubiquitin Q41N at different pressures relative to those at 1 bar (pH 4.0 and 278 K) (broken line, residues 23, 31, and 40 preferentially losing intensity).

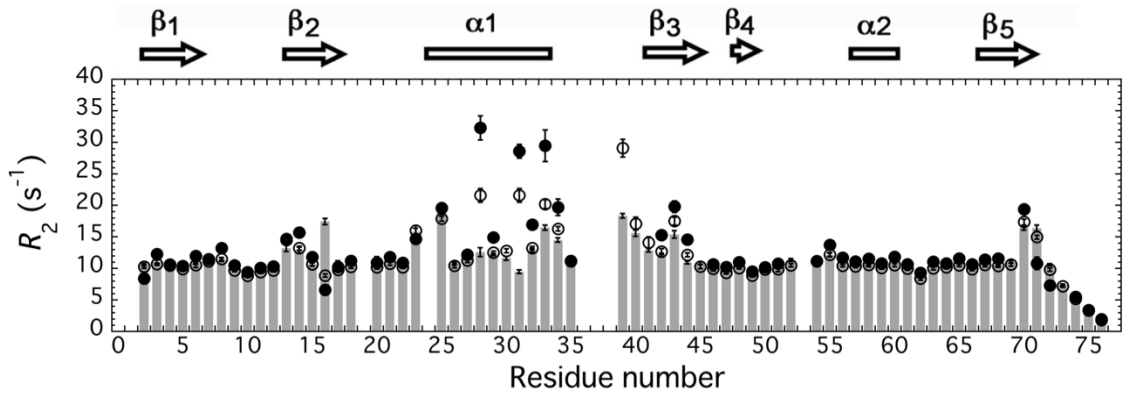

Figure 3. Pressure dependence of ^{15}N-transverse relaxation rate constants. ^{15}N-transverse relaxation rate constants, R_2, determined for uniformly ^{15}N-labeled ubiquitin Q41N at different pressures (bars, 1 bar; open circles, 1000 bar; closed circles, 2500 bar) at pH 4.0 and 278 K. Error bars show the root-mean-square-deviation obtained from the single exponential fit. Secondary structure elements are indicated at the top of the panel by bars (α-helices) and arrows (β-strands).

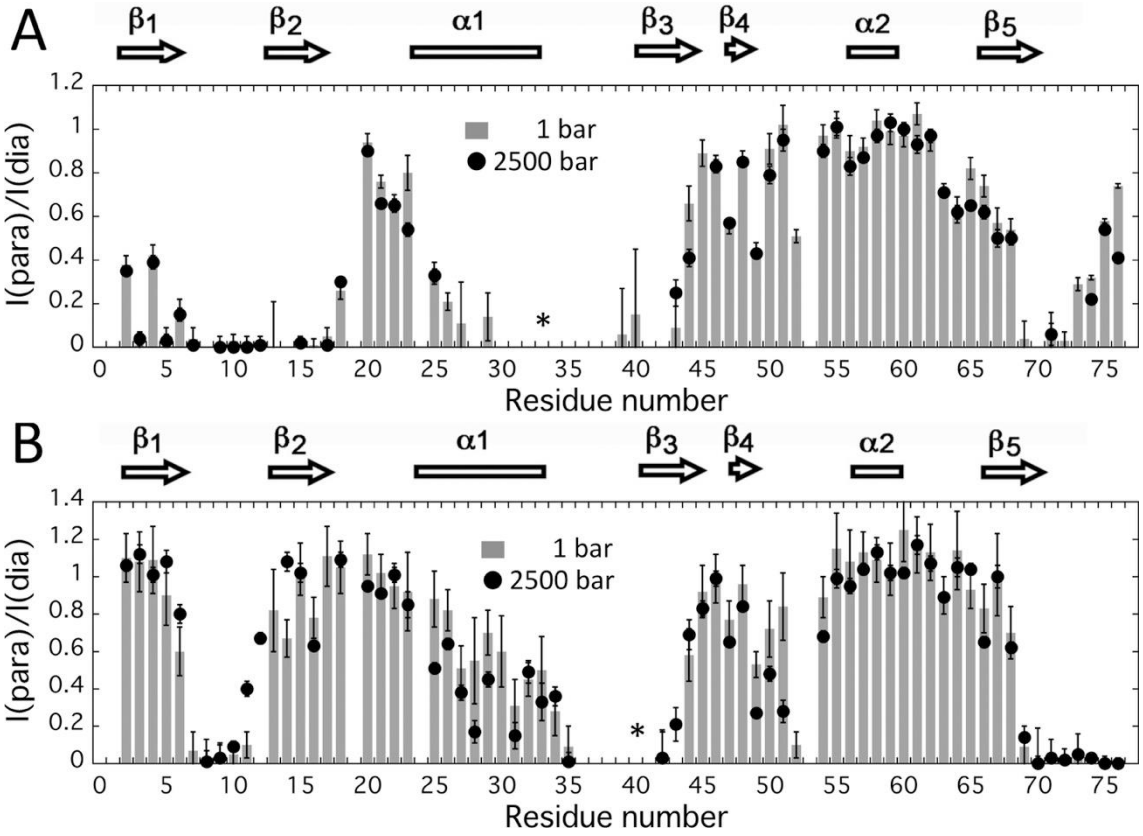

Figure 4. PRE effects for ubiquitin K33C/Q41N and ubiquitin Q40C/Q41N. Ratios of peak heights between paramagnetic and diamagnetic samples (I_{para}/I_{dia}) of ubiquitin K33C/Q41N (A) and ubiquitin Q40C/Q41N (B) at 1 bar (bars) and 2500 bar (closed circles). Secondary structure elements are indicated at the top of the panel by bars (α-helices) and arrows (β-strands). Asterisks show the sites of MTSL covalent attachment. The error bars for I_{para}/I_{dia} were estimated from the noise considering error propagation, i.e. $\Delta\left({I_{para}}/{I_{dia}}\right) = \left({I_{para}}/{I_{dia}}\right)\sqrt{\left(\frac{\Delta I_{para}}{I_{para}}\right)^2 + \left(\frac{\Delta I_{dia}}{I_{dia}}\right)^2}$.

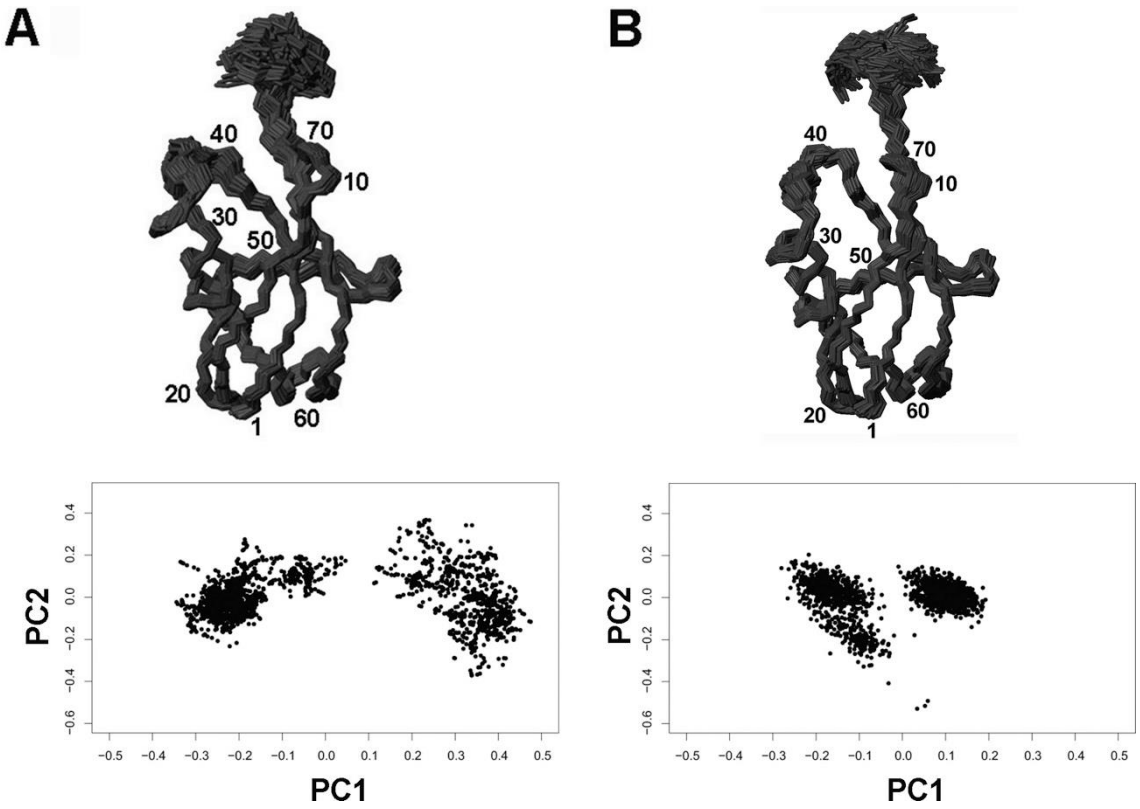

Figure 5. NMR structure refinement based on Bayesian inference. (A and B) (top) The 1900 structures yielded by the Bayesian-refined method without and with PRE-based structural restraints, respectively. (bottom) Distributions of the first and second principal components (PC1, PC2) for the structural ensembles shown in the top panel. PCA was performed for the Cα atoms of residues 1–70. 20 energy-minimized structural models were deposited in the Protein Data Bank (ID: 6K4I).

Acknowledgements
This work was supported by JSPS KAKENHI Grant Number 25840025 to R. K. This work was performed in part using the NMR spectrometer with the ultra-high magnetic fields under the Collaborative Research Program of Institute for Protein Research, Osaka University.

Author contributions
The manuscript was written by R.K. NMR measurements and structural determination were performed by T. W., T. I., S. K., N. B, M. W., and R. K. All authors reviewed the manuscript.

Competing interests: The authors declare no competing interests.

Data deposition
20 energy minimized models were deposited in the Protein Data Bank (ID: 6K4I). Chemical shift data and structural restraints are available in the Biological Magnetic Resonance Bank (ID: 36241).